Thermochemical interpretation of 1-D seismic data for the lower mantle : The significance of nondiabatic thermal gradients and compositional heterogeneity

L. Cobden, S. Goes, M. Ravenna, E. Styles, F. Cammarano, Kerry Gallagher, J.A.D Connolly

Thermochemical interpretation of 1-D seismic data for the lower mantle: The significance of nonadiabatic thermal gradients and compositional heterogeneity

Laura Cobden,[1,2] Saskia Goes,[1] Matteo Ravenna,[1] Elinor Styles,[1] Fabio Cammarano,[3] Kerry Gallagher,[4] and James A. D. Connolly[5]

Received 17 December 2008; revised 26 June 2009; accepted 19 August 2009; published 26 November 2009.

[1] Equation-of-state (EOS) modeling, whereby the seismic properties of a specified thermochemical structure are constructed from mineral physics constraints, and compared with global seismic data, provides a potentially powerful tool for distinguishing between plausible mantle structures. However, previous such studies at lower mantle depths have been hampered by insufficient evaluation of mineral physics uncertainties, overestimation of seismic uncertainties, or biases in the type of seismic and/or mineral physics data used. This has led to a wide, often conflicting, variety of models being proposed for the average lower mantle structure. In this study, we perform a thorough reassessment of mineral physics and seismic data uncertainties. Uncertainties in both the type of EOS, and mineral elastic parameters, used are taken into account. From this analysis, it is evident that the seismic variability due to these uncertainties is predominantly controlled by only a small subset of the mineral parameters. Furthermore, although adiabatic pyrolite cannot be ruled out completely, it is problematic to explain seismic velocities and gradients at all depth intervals with such a structure, especially in the interval 1660–2000 km. We therefore consider a range of alternative thermal and chemical structures, and map out the sensitivity of average seismic velocities and gradients to deviations in temperature and composition. Compositional sensitivity is tested both in terms of plausible end-member compositions (e.g., MORB, chondrite), and via changes in each of the five major mantle oxides, SiO_2, MgO, FeO, CaO, and Al_2O_3. Fe enrichment reduces both *P* and *S* velocities significantly, while Si enrichment (and Mg depletion) increases *P* and *S* velocities, with a larger increase in *P* than in *S*. Using purely thermal deviations from adiabatic pyrolite, it remains difficult to explain simultaneously all seismic observations. A superadiabatic temperature gradient does improve the seismic fit in the lowermost mantle, but should be accompanied by concurrent bulk chemistry changes. Our results suggest that the most plausible way to alter bulk chemistry in the lowermost mantle, simultaneously fitting density, bulk velocity and shear velocity constraints, is an increasing contribution of a hot, basalt-enriched component with depth.

Citation: Cobden, L., S. Goes, M. Ravenna, E. Styles, F. Cammarano, K. Gallagher, and J. A. D. Connolly (2009), Thermochemical interpretation of 1-D seismic data for the lower mantle: The significance of nonadiabatic thermal gradients and compositional heterogeneity, *J. Geophys. Res.*, *114*, B11309, doi:10.1029/2008JB006262.

1. Introduction

[2] The Adams-Williamson equation [*Williamson and Adams*, 1923] describes the relationship between density and depth for a homogeneous, adiabatic, self-compressing layer. *Birch* [1952] used this equation to compare the elastic moduli of the mantle (as calculated from the velocity profiles of *Jeffreys and Bullen* [1940]) with those derived from experimental compression of a range of solids at lower mantle pressures. As the two sets of values were similar, Birch argued that the lower mantle must be "reasonably homogeneous" with at most only small deviations from adiabaticity. Furthermore, when normal mode measurements have been used to constrain the density profile of the mantle, only minor deviations from the Adams-Williamson equation are required [*Dziewonski and Anderson*, 1981]. Thus to first order it would seem that the lower mantle can be represented by a chemically homogenous, adiabatic material.

[1]Department of Earth Science and Engineering, Imperial College London, London, UK.
[2]Now at Department of Earth Sciences, Utrecht University, Utrecht, Netherlands.
[3]Institute of Geophysics, ETH Zurich, Zurich, Switzerland.
[4]Géosciences Rennes, Université de Rennes 1, Rennes, France.
[5]Institute of Mineralogy and Petrography, ETH Zurich, Zurich, Switzerland.

0148-0227/09/2008JB006262$09.00

[3] However, geochemistry presents compelling evidence for compositional heterogeneity at depth in the mantle. Most fundamentally, the 60000 km long global mid-ocean ridge network produces basalts which are remarkably uniform in chemical composition, yet the volcanism at oceanic islands generates basalts presenting a diverse range of compositions which can differ strongly from both each other, and the mid-ocean ridge basalts [*Hofmann*, 1997]. The classic interpretation of this phenomenon is that mid-ocean ridge basalts (MORBs) derive from a laterally homogeneous upper mantle source region, whereas the ocean island basalts (OIBs) come from separate, chemically distinct reservoirs (although other interpretations exist [e.g., *Anderson*, 2007]). The key issue is then where to put these chemically distinct regions within the mantle, and whether they can be detected seismically.

[4] Trace element patterns and isotopic signatures, notably enrichment in incompatible and volatile elements relative to MORB, suggest OIB reservoirs are either chemically primitive [e.g., *Trieloff et al.*, 2000], i.e., undisturbed by earlier melting events or convective mixing, and/or derive from recycled subducted crust [e.g., *Rapp et al.*, 2008]. Until the mid-1990s, it was often assumed, on the basis of cosmochemical and mass balance constraints, that the entire mantle below 660 km was, convectively and chemically, largely isolated from the upper mantle [e.g., *Hart and Zindler*, 1986]. Under this scenario, OIBs were primitive melts transported from the lower mantle by thermal plumes. However, seismic tomography has repeatedly indicated that subducting slabs penetrate the lower mantle, with some slabs traveling as far down as the core-mantle boundary [*Grand et al.*, 1997; *van der Hilst et al.*, 1997]. This rules out the possibility of complete isolation between upper and lower mantle.

[5] A number of "hybrid" solutions have been proposed to reconcile the seismic and geochemical observations, and an emerging popular scenario is to place a compositionally distinct region, or regions, somewhere in the bottom 1000 km of the mantle [*Albarede and van der Hilst*, 2002; *Kellogg et al.*, 1999; *van der Hilst and Karason*, 1999]. Numerical modeling indicates that both primitive and recycled mantle components can become concentrated deep within the lower mantle, as piles, undulating layers, or blobs [*Kellogg et al.*, 1999; *Nakagawa and Tackley*, 2004], via chemically driven density variations. Such chemically enriched regions provide a suitable source for OIBs, satisfying available geochemical constraints. Additionally, this scenario is consistent with seismic observations, namely the existence of "superplumes" beneath Africa and the central Pacific. Superplumes, or LLSVPs ("large, low shear velocity provinces"), are long-wavelength tomographic anomalies below ~2000 km depth, characterized by low *P* and *S* velocities [*Su and Dziewonski*, 1997]. When their *P* and *S* velocities are expressed as bulk sound (K/ρ) and shear (G/ρ) velocities, a negative correlation is observed [*Ishii and Tromp*, 1999; *Kennett et al.*, 1998; *Masters et al.*, 2000; *Resovsky and Trampert*, 2003; *Saltzer et al.*, 2001; *Su and Dziewonski*, 1997], with high bulk velocities and low shear velocities. This anticorrelation is indicative of a chemical, as opposed to purely thermal, origin for the superplumes [e.g., *Trampert et al.*, 2004].

[6] Equation-of-state (EOS) modeling, whereby the seismic properties of theoreticized mantle structures are computed from mineral physics data, has been invoked on many occasions as a tool for discriminating between the various thermochemical possibilities for the lower mantle (e.g., most recently *Aizawa and Yoneda* [2006], *Cammarano et al.* [2005b], *da Silva et al.* [2000], *Deschamps and Trampert* [2004], *Jackson* [1998], *Khan et al.* [2008], *Li and Zhang* [2005], *Matas et al.* [2007], *Mattern et al.* [2005], and *Trampert et al.* [2001]). However, these studies have drawn widely varying interpretations as to whether a chemically homogeneous, near-adiabatic structure does or does not fit global seismic data, and what the nature of any alternative structure could be. Such inconsistencies arise through the authors' choice of specific mineral elastic parameters; the method of extrapolating those parameters to lower mantle conditions; and the nature of the seismic data against which the thermochemical models are compared. In particular, as we will show, there has been a tendency to underestimate (or disregard) mineral physics uncertainties, and to overestimate (or disregard) seismic data uncertainties. Because of the limited availability of relevant data, some studies have restricted calculations to the FeO-MgO-SiO_2 system, thereby excluding the effects of CaO and/or Al_2O_3, while other studies have considered only bulk sound velocities, neglecting the potential importance of shear moduli effects.

[7] In this study, EOS modeling of the lower mantle is revisited, to include a thorough assessment of both elastic parameter and EOS extrapolation uncertainties, referenced to a tightly constrained seismic data set. A range of thermal and chemical structures based on the CaO-FeO-MgO-Al_2O_3-SiO_2 (CFMAS) system are tested against *P* and *S* velocities simultaneously. The purpose of this is twofold: first, to map out the sensitivities of *P* and *S* velocities to thermal and chemical changes, and second to evaluate the extent to which the mineral physics data currently allow us to discriminate between different thermochemical models for the lower mantle.

2. Data and Uncertainties

[8] Our study considers the lower mantle from 800 km to 2500 km, i.e., from below the completion of garnet-to-perovskite phase transitions, and terminating above the seismically complex D″ layer. This depth range is also above the likely depth of the perovskite-to-postperovskite phase transition [e.g., *Ohta et al.*, 2008]. Using several EOSs, we calculate average *P* and *S* wave velocities and velocity gradients in five depth intervals: 800–920 km, 920–1200 km, 1200–1660 km, 1660–2000 km and 2000–2500 km, and compare the values for our models with those obtained from inversion of real seismic data.

2.1. Seismic Data

[9] Lower mantle 1-D seismic structure is very tightly constrained by seismic data. It is therefore not necessary to test models directly against the raw data, i.e., *P* and *S* arrival times (as has been the case for the upper mantle where seismic uncertainties are larger [e.g., *Cammarano et al.*, 2005a; *Cobden et al.*, 2008]). Instead we can facilitate comparisons by determining the fit of models to average velocities and velocity gradients, which are simpler to interpret than the corresponding travel times.

[10] We use average velocities and gradients inferred from the 1-D seismic reference models PREM [*Dziewonski and Anderson*, 1981] and AK135 [*Kennett et al.*, 1995] and

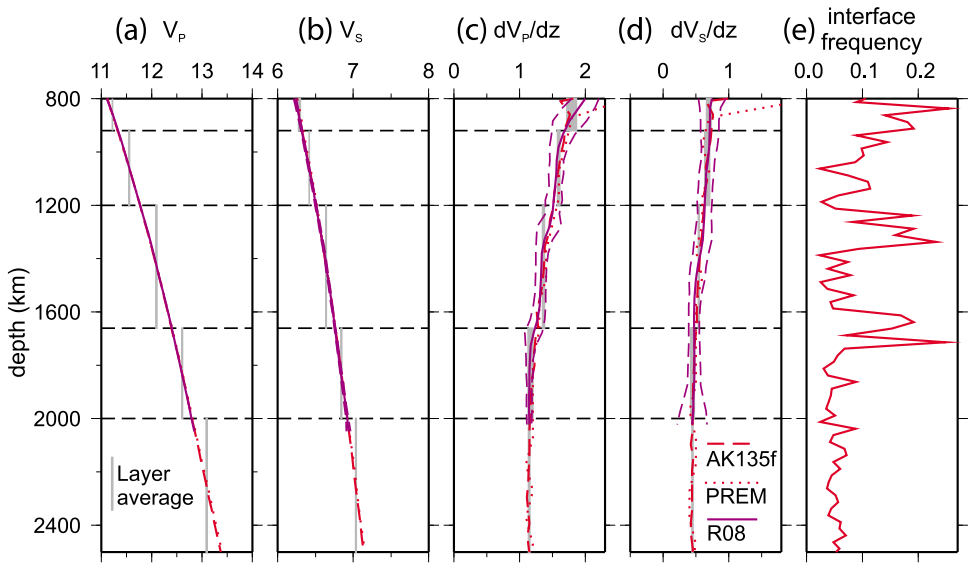

Figure 1. Seismic data used in this study. Solid purple line (R08) is the output from our first inversion, in which the number of layers in the velocity model is allowed to vary. Dashed purple lines indicate 95% confidence bounds. Figure 1e shows the frequency with which layer interfaces occurred at each depth during this part of the inversion (which was run with four different starting models). There are no sharp peaks indicating no unambiguous discontinuities in the lower mantle, i.e., a very smooth structure. Hence the depths at which to place the layer interfaces are flexible but have been chosen to correspond broadly with where the interface frequencies are highest (black dashed lines). Grey vertical bars show average velocities and gradients obtained with fixed layer interfaces during the second inversion and subsequently used for comparison with thermochemical models.

run our own inversion of global ISC traveltime data [*Engdahl et al.*, 1998; E. R. Engdahl, personal communication, 2000] to determine the uncertainties on the seismic data. In this inversion, the lower mantle is parameterized as a series of layers, within which velocity gradients are constant, such that *P* and *S* velocities are specified only at the interfaces between layers. A starting velocity model is chosen, and a Reversible Jump Markov Chain Monte Carlo algorithm [after *Green*, 1995] (see Appendix A) is applied. This fully nonlinear algorithm has the flexibility of allowing both the number of layers and the depths of layer interfaces to vary (i.e., the dimensions of the model can change during the inversion), as well as the velocities at the interfaces. At each iteration of the inversion, the fit of a given velocity model to direct *S* and *P* arrival times is assessed using the ray-tracing code TauP [*Crotwell et al.*, 1999].

[11] Initially, the inversion was run to allow for changes in all three of the parameter types: layer depths, number of layers, and interface velocities. The purpose of this was to try to establish where in the lower mantle any interfaces that separate regions of distinct velocity gradients may occur. However, it was found that both the number and depths of such interfaces varied between different runs of the inversion, emphasizing the smooth, continuous nature of the lower mantle velocity profile (Figure 1), especially between 1200 and 1800 km. Nonetheless, most inversion runs suggested three main interfaces: one between 800 and 900 km, another between 1100 and 1200 km, and a third at ~1600–1800 km.

[12] Following this, we reran the inversion code, but with the layer interfaces kept fixed at 760 km, 920 km, 1200 km, 1660 km and 2000 km, so that only the velocities at the interfaces were inverted for. These velocities then provided the average velocities and gradients used in this study to constrain mantle structure.

[13] 95% of the velocity models output from this procedure lie within an uncertainty bound of ±0.01 km/s between 800 and 2000 km, while the velocity gradients have uncertainties of up to $\pm 3 \times 10^{-5}$ s^{-1}. This is similar to the uncertainty of ±0.02 km/s assigned to the velocities in AK135 by *Kennett et al.* [1995], and equates to a maximum percentage error of ±0.09% on V_P and ±0.16% on V_S. This is significantly less than the uncertainty of ~0.5–1% typically allocated to lower mantle seismic structure, in those studies in which seismic uncertainties are taken into consideration [e.g., *Cammarano et al.*, 2005b; *Deschamps and Trampert*, 2003; *Deschamps and Trampert*, 2004].

[14] On Figures 1, 2, 5, 6, and 7, we show the velocities and velocity gradients output from two separate runs of the inversion, based on different starting models. We also show values computed for PREM and AK135, the former being derived from a joint inversion of traveltimes and normal modes, and the latter from inversion of traveltimes only. The difference between values obtained from our inversion, and the reference models AK135 and PREM, gives an indication of the total error bars on the seismic structure.

[15] Below 2000 km, our inversion does not have resolution to *S* velocity structure. This is because the inversion uses direct arrivals only, and the direct *S* phase is complicated by overlap with the *SKS* arrival in the lowermost mantle. Therefore for the interval 2000–2500 km, average velocities and velocity gradients are shown for PREM and AK135 only; hence the uncertainty bounds are less clearly defined than at shallower depth intervals, although our

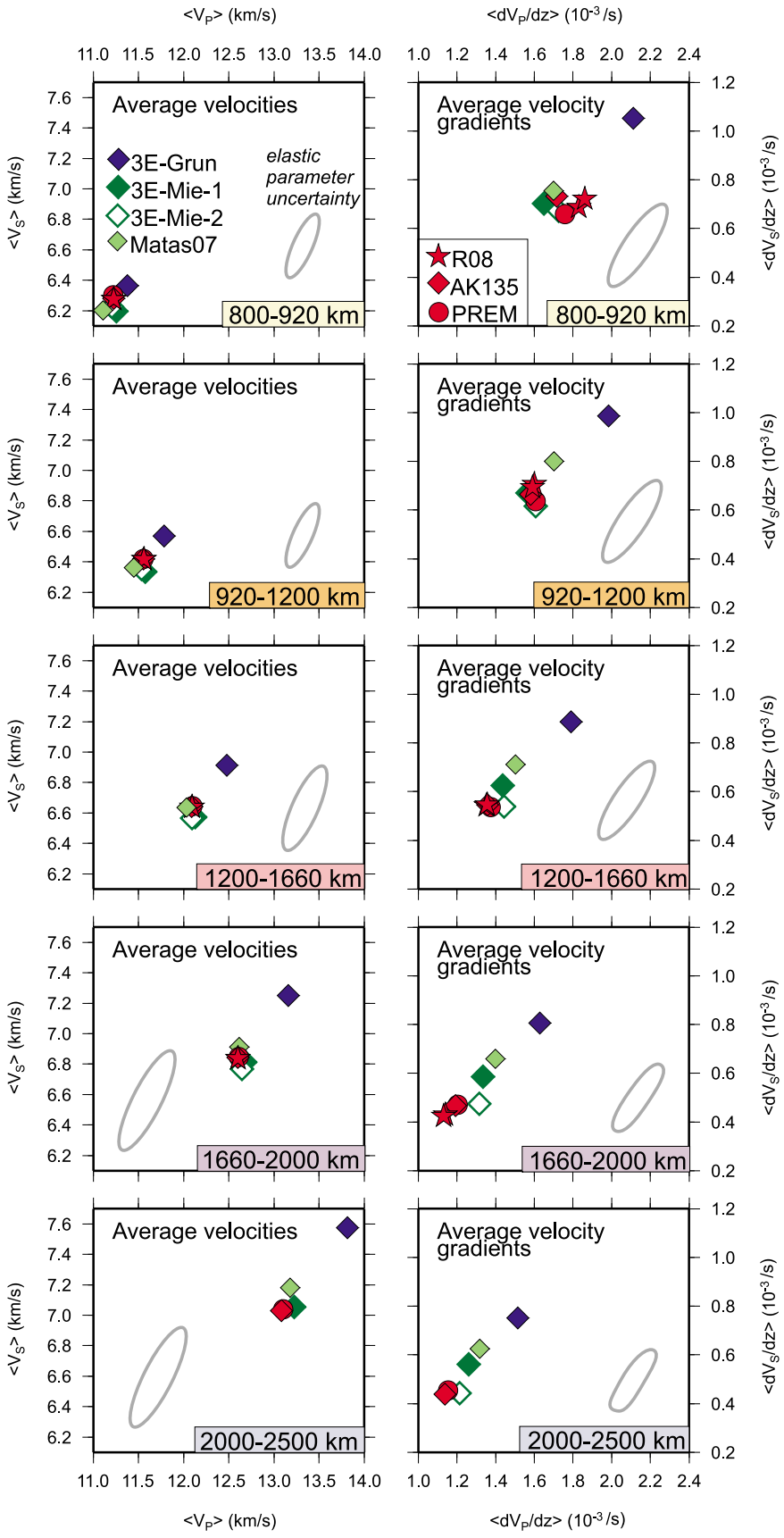
<V_P> (km/s)
<dV_P/dz> (10^-3 /s)
<V_S> (km/s)
<dV_S/dz> (10^-3 /s)
Average velocities
Average velocity gradients
3E-Grun
3E-Mie-1
3E-Mie-2
Matas07
elastic parameter uncertainty
R08
AK135
PREM
800-920 km
920-1200 km
1200-1660 km
1660-2000 km
2000-2500 km

Figure 2

inverted P velocities for 2000–2500 km indicate uncertainties similar to those between 1660 and 2000 km.

2.2. Equation of State

[16] There is no clear consensus on what is the most suitable equation of state for modeling the lower mantle. The most commonly used pressure extrapolation is the third-order Birch-Murnaghan formulation, in which Helmholtz free energy is expressed as a Taylor series expansion of finite strain, truncated to third order (see, e.g., *Jackson* [1998] for a detailed review). An investigation by *Jackson* [1998] has indicated that it does not matter whether the pressure extrapolation is done along an adiabat or along an isotherm. However, it has been suggested that expansion of the Birch-Murnaghan approach to fourth order may be more appropriate under lower mantle conditions [*Davies and Dziewonski*, 1975]. Meanwhile, two main approaches for high temperature extrapolation can be found in the geophysical literature. The first, associated with isentropic (adiabatic) pressure extrapolation, uses an Anderson-Gruneisen temperature correction. This is the method favored by *Trampert et al.* [2001] and *Deschamps and Trampert* [2004], as well as being that adopted by *Cammarano et al.* [2005b]. It is endorsed [e.g., *Trampert et al.*, 2001] because it fits measured data for MgO [*Anderson et al.*, 1995] extremely closely. However, *Deschamps and Trampert* [2004] found that unless a cross-derivative term for the shear modulus, i.e., $\partial^2 G/\partial P \partial T$, is incorporated into the EOS then the extrapolation does not agree with values of the shear modulus of Mg perovskite obtained from ab initio simulations. Precise values for the cross-derivatives of K and G have not yet been determined. For this reason, some researchers [e.g., *Matas et al.*, 2007] favor the second temperature extrapolation approach which, used in conjunction with an isothermal pressure extrapolation, involves a Mie-Gruneisen temperature correction (outlined by *Matas et al.* [2007 and references therein]). With this method, cross derivatives are accounted for internally and self-consistently.

[17] We therefore consider three different equations of state: a third-order Birch-Murnaghan pressure extrapolation with nonlinear Gruneisen temperature correction (method 3E-Grun-4 of *Cobden et al.* [2008]); a fourth-order Birch-Murnaghan pressure extrapolation with Gruneisen temperature correction (method 4E-Grun); and a modified third-order finite strain isothermal pressure extrapolation with Mie-Gruneisen temperature correction (method 3E-Mie of *Cobden et al.* [2008]). For method 3E-Mie, two variants are considered: 3E-Mie-1 is based on the EOS of *Stixrude and Lithgow-Bertelloni* [2005a] while 3E-Mie-2 uses a modified version of this EOS [*Stixrude and Lithgow-Bertelloni*, 2005b]. The aim of using these three EOSs is first to determine how significant the shortcomings of the 3E-Grun thermal extrapolation are seismically relative to the 3E-Mie approach, i.e., once they are translated into actual velocities, and second whether it is actually possible to fit adiabatic pyrolite to seismic data, once uncertainties in EOS are taken into account in addition to the mineral parameter uncertainties.

2.3. Elastic Parameter Uncertainties

[18] Even greater controversy exists for deciding which values of particular elastic parameters should be applied with a given EOS than for the choice of EOS itself. This is because either the parameters are unknown/poorly indicated by experimental data, or different experiments produce vastly different results [*Matas et al.*, 2007]. Such controversy has led to widely varying results as to whether an adiabatic temperature gradient and/or pyrolitic composition do or do not fit seismological data for the lower mantle (*Aizawa and Yoneda* [2006], *Jackson* [1998], *Matas et al.* [2007], and *Mattern et al.* [2005] all use the same equation of state but between them cite evidence for an adiabatic pyrolite mantle, a subadiabatic thermal structure, a superadiabatic thermal structure, Si enrichment with depth, Fe enrichment with depth, and Mg enrichment with depth). In particular, it is clear that seismic velocities are highly sensitive to the pressure derivative of the shear modulus, but there is significant disagreement between experimentally determined values (*Matas et al.* [2007] provide a good review of the topic).

[19] The advantage of the approach presented here over previous studies of the lower mantle is that we consider uncertainties in both the EOS and the mineral elastic parameters. A careful consideration of elastic parameter uncertainties for the FeO-MgO-SiO_2 system, and in later studies also CaO, was previously performed by Trampert and coworkers [*Trampert et al.*, 2001; *Deschamps and Trampert*, 2003, 2004], and similarly, elastic moduli uncertainties were assessed in detail for the CaO-FeO-MgO-Al_2O_3-SiO_2 system by *Cammarano et al.* [2005b]. However, these studies used a specific EOS which differs in its temperature extrapolation from that favored by more recent studies [e.g., *Khan et al.*, 2008; *Matas et al.*, 2007], and in our study we consider both these variants of EOS. Uncertainties in all the elastic parameters are taken into account simultaneously, and mapped as an uncertainty contour in velocity space. Adiabatic pyrolite can only be conclusively discounted as a plausible average structure for the lower mantle if it falls outside this uncertainty contour.

[20] For 3E-Grun and 4E-Grun, 5000 models were calculated for which the parameters K, G, $\partial K/\partial T$, $\partial G/\partial T$, $\partial K/\partial P$, $\partial G/\partial P$; and thermal expansion coefficient α varied randomly within the uncertainty bounds defined by *Cammarano et al.* [2003], using a Monte Carlo search of the solution space, for the minerals $MgSiO_3$ perovskite and MgO periclase. Previous studies have indicated that 5000 models is a sufficiently large sample to define the solution space [*Cammarano et al.*, 2005b; *Cobden et al.*, 2008]. Random values were not assigned to the elastic parameters of Ca perovskite because

Figure 2. Fit of adiabatic pyrolite to seismic data using different EOSs between 800 and 2500 km. Grey ellipse is 95% contour for 5000 models with randomly varying elastic parameter uncertainties (uncertainties defined by *Cammarano et al.* [2003]), calculated with method 3E-Grun. For comparison, the adiabatic pyrolite of *Matas et al.* [2007] is plotted. This was computed using a third-order Birch-Murnaghan pressure extrapolation and Mie-Gruneisen temperature extrapolation (i.e., 3E-Mie). The differences between the velocities from our own seismic inversion (R08) and from AK135 and PREM indicate the amount of uncertainty on the seismic data. Note that P and S are not plotted to the same scale.

it is probable that its uncertainties are encapsulated by those defined with the other two minerals. For 4E-Grun, the second order derivatives of K and G were varied by up to -200% from their starting values.

[21] For 3E-Mie-1, elastic parameter values are taken from the thermodynamic database of *Stixrude and Lithgow-Bertelloni* [2005a] supplemented by data for the lower mantle as described by *Khan et al.* [2006]. Meanwhile, the 3E-Mie-2 calculations use the updated thermodynamic database published by *Stixrude and Lithgow-Bertelloni* [2007] implemented in the program Perple_X [*Connolly*, 1990]. However, uncertainty bounds on individual parameters are given by *Stixrude and Lithgow-Bertelloni* [2007] for method 3E-Mie-2 only. For computational efficiency, we calculated velocity models for which each of the elastic parameters took their maximum and minimum values only. From these tests, we found that uncertainties from different parameters are broadly additive. For example, higher values of K and $\partial K/\partial P$ will both increase V_P, and the increase observed with setting both K and $\partial K/\partial P$ to their maximum values is greater than that observed from just setting one of them to its maximum. For S velocities, the highest values are obtained by setting K, $\partial K/\partial P$, G, $\partial G/\partial P$ to their maximum values within the uncertainty bounds, and η to its minimum where η is a parameter describing the temperature dependence of the shear modulus [see, e.g., *Stixrude and Lithgow-Bertelloni*, 2005b]. P velocities are only significantly altered by two parameters: K and $\partial K/\partial P$ (highest velocities occurring when these are set to their maximum values, and vice versa) and the magnitude of such variations are less than those for S waves. Interestingly the effects of elastic parameters on velocity gradients are not correlated to the effects on velocities: P velocity gradients are only altered significantly by changes in K, and this time the minimum value of K produces the highest gradient. S velocity gradients are only significantly affected by $\partial G/\partial P$, with the highest gradients occurring at the maximum value of $\partial G/\partial P$. The seismic error bounds derived from this method are very similar in magnitude to those defined by the extensive Monte Carlo search. Therefore, in Figure 2, the velocity space mapped out by elastic parameter uncertainties is illustrated as a single elliptical contour, this contour being the locus of the 95% confidence limit of the 5000 random models.

[22] Certain features of the uncertainty ellipses require some discussion. First, it appears that the velocity gradient uncertainties become smaller with increasing depth (see Figure 2), which is counterintuitive with the notion that uncertainties should increase the further they are extrapolated from room temperature and pressure. This happens for uncertainty bounds estimated with both the 3E-Grun and 3E-Mie data sets. However, the absolute values of the gradients also decrease, so that in fact the percentage uncertainty remains almost constant as the depth increases. The lack of an increase may be related to the small number of minerals present and the similarity of their bulk and shear moduli as P and T increase. Second, uncertainties in V_S are at times a little larger than uncertainties in V_P. This is probably a consequence of the sensitivity of V_S to a greater range of elastic moduli than V_P.

2.4. Phase Equilibria

[23] Phase relations along a given P-T locus are calculated using the Perple_X program package [*Connolly*, 1990, 2005] via a free-energy minimization algorithm. For methods 3E-Grun, 4E-Grun and 3E-Mie-1 the input thermodynamic data for the minimization are from *Stixrude and Lithgow-Bertelloni* [2005a] supplemented in places as described by *Khan et al.* [2006], and for 3E-Mie-2, the input data are taken from *Stixrude and Lithgow-Bertelloni* [2007]. Bulk compositions are specified in terms of the end-members SiO_2, MgO, FeO, CaO and Al_2O_3. Partitioning of Fe between the different minerals present is determined implicitly by the free energy minimization.

2.5. Effect of Anelasticity

[24] In the upper mantle, the contribution of (shear) anelasticity to seismic velocities is significant [*Karato*, 1993]. However, studies of the lower mantle indicate that the importance of anelasticity is considerably smaller below the transition zone [*Brodholt et al.*, 2007; *Cammarano et al.*, 2003; *Matas and Bukowinski*, 2007; *Trampert et al.*, 2001]. Therefore, the anharmonic velocities we calculate are corrected for anelasticity, but the same anelasticity structure is assumed in all our models (model Q5 of *Cammarano et al.* [2003]).

3. Fit of 1300°C Adiabatic Pyrolite to Seismic Data

[25] We would like to test whether a compositionally homogeneous, thermally well-mixed lower mantle is compatible with seismic data. We begin by assuming a composition of pyrolite (i.e., MORB source, as expected for whole mantle convection) and an adiabatic temperature gradient (as results from vigorous convection). Preliminary investigations by *Cammarano et al.* [2005b] indicated that, for a pyrolitic composition, and an adiabat with potential temperature of 1300°C, a chemically homogeneous, adiabatic structure is not compatible with seismic data. In particular, calculated model velocities of *Cammarano et al.* [2005b] increase too rapidly with depth compared with 1-D seismic reference models. However, the computations of *Cammarano et al.* [2005b] do not consider uncertainties in the equation of state (EOS) used to compute lower mantle velocities. The precise choice of EOS used is more pertinent in the lower mantle than for the upper mantle, since mineral parameters are being extrapolated much further from their experimental values, leading to greater potential for errors.

[26] Additionally, an adiabatic, homogeneous structure need not have to be pyrolitic in composition, or constrained to a potential temperature of 1300°C. Furthermore, within a vigorously convecting, chemically homogeneous system, internal heating can lead to subadiabatic temperature gradients [*Bunge et al.*, 2001]. In fact, given the evidence for thermochemical heterogeneity in the upper mantle [*Cobden et al.*, 2008], it seems especially likely that the physical structure represented by 1-D seismic models will deviate from 1300°C adiabatic pyrolite.

[27] In Figure 2 we show the fits of the different EOSs 3E-Grun and 3E-Mie to average velocities and velocity gradients of the lower mantle, for 1300°C adiabatic pyrolite. Method 3E-Grun, the EOS used by *Cammarano et al.* [2005b], tends toward being too fast, and having too high velocity gradients, at all depth intervals, but with increasing depth it deviates further from the seismic data. In fact, it

deviates so far from the seismic data that even extreme adjustments in temperature and composition (not plotted here) cannot bring its velocities and gradients to be in line with the data. We conclude that, irrespective of whether adiabatic pyrolite is an appropriate structure for the lower mantle, the 3E-Grun EOS is not suitable for modeling lower mantle behavior. Likewise, the fourth-order EOS, 4E-Grun, is rejected as a useful EOS to model the lower mantle because it overestimates the second derivative of the velocities, such that nearly all of the 5000 models develop negative velocity gradients above 2500 km. This is probably related to the fact that the second order pressure derivatives of the elastic moduli, $\partial^2 K/\partial P^2$ and $\partial^2 G/\partial P^2$, which the fourth-order EOS requires, are not available for most minerals.

[28] Method 3E-Mie has a much closer fit to the seismic data. Taking elastic parameter uncertainties into account, it could be argued that with 3E-Mie, 1300°C adiabatic pyrolite is consistent with the average velocities at all depth intervals. For the average velocity gradients, the only depth interval where 3E-Mie does not fit the seismic data is 1660–2000 km, because the P velocity gradients are too high. However, 3E-Mie-1 and 3E-Mie-2 both use elastic parameter data sets which at times lie at one extreme of the published data range. We have therefore added to Figure 2 the adiabatic pyrolite calculated by *Matas et al.* [2007], which uses the same style of EOS as 3E-Mie but a different mineral physics data set. The mineral parameters from *Matas et al.* [2007] are more average relative to a range of other studies that have noted systematic mismatches between predicted adiabatic pyrolite velocities and seismic models. This extra data point ("Matas07," Figure 2) yields average velocities and gradients intermediate between those of 3E-Mie and 3E-Grun such that it fits the average velocities, but with increasing depth both its P and S gradients become increasingly too high.

[29] We conclude that using a Mie-Gruneisen temperature correction (method 3E-Mie) provides a much closer fit to lower mantle 1-D seismic data than a simple Gruneisen correction (method 3E-Grun and the method of *Cammarano et al.* [2005b]), for both P and S velocities. Adiabatic pyrolite may fit the seismic data, but there is still a tendency for velocities and velocity gradients to be overestimated with increasing depth, and in particular it is difficult to fit P velocity gradients between 1660 and 2000 km. This result is consistent with experimental measurements and first principles simulations of sound velocities in perovskite and magnesiowustite, which have noted that V_P and V_S of pyrolitic compositions are too high to match seismic data at these depths [*Jackson et al.*, 2006; *Wentzcovitch et al.*, 2004].

4. Alternative Thermochemical Structures

[30] Unlike the upper mantle, P and S velocities of 1-D seismic reference models increase smoothly with depth in the lower mantle, with no major discontinuities (Figure 1). Phase diagram computations indicate that behavior is dominated by just three minerals: orthorhombic Mg/Fe/Al perovskite; cubic Ca perovskite; and Fe/Mg magnesiowustite, whose proportions do not vary with depth for a fixed chemical composition. Any volumetrically significant deviations in temperature, composition or structure must therefore be relatively subtle and/or nonglobal in character in order that they bias the 1-D average seismic signal, without producing global discontinuities. The purpose of this section is to test the magnitude and direction in which alternative temperature structures and compositions can alter the 1-D average seismic signal, to see if any would provide an improved fit to the seismic data over adiabatic pyrolite.

4.1. Alternative Thermal Structures

[31] Birch demonstrated that deviations from adiabaticity in the lower mantle are likely to be small [*Birch*, 1952]. Nonetheless, a range of mechanisms could allow either subadiabatic or superadiabatic gradients to develop which, although small, could influence the 1-D seismic average. Additionally, if thermal changes are concurrent with chemistry changes, then the latter may mask the seismic effect of the former. In fact, the temperature of the lower mantle is only loosely constrained at two points: the 660 discontinuity, and the core-mantle boundary (Figure 3). This leaves a lot of leeway for deviations from adiabaticity.

[32] Numerical simulations of convection in the Earth have repeatedly shown that internal heating due to radioactive decay within the mantle causes temperature to increase with depth more slowly than that predicted for an adiabat, i.e., subadiabaticity [*Bunge et al.*, 2001]. Subadiabatic gradients may also develop as rising hot flows (/sinking cold flows) are forced to turn from vertical to horizontal at the top and base of the mantle [*Sinha and Butler*, 2007]. This subadiabaticity can amount to several hundred degrees by the base of the mantle.

[33] Alternatively, chemical changes in the lowermost mantle could impede convective flow. For example, stagnation of hot material could occur at depth if there is enrichment of iron, as this has a high intrinsic density compared with iron-poor compositions. (Under lower mantle conditions, chemical buoyancy can potentially dominate over thermal buoyancy, because thermal expansion is greatly reduced at high pressures [*Trampert et al.*, 2004]). Or, the discovery of a high-spin to low-spin transition in iron itself around 1700–2000 km depth [*Badro et al.*, 2003] provides a means of enhancing thermal conductivity, in turn reducing convective overflow [*Badro et al.*, 2005]. Either of these effects may contribute to a superadiabatic temperature gradient at depth. Additionally, a deep, dense layer enriched in heat-producing (radioactive) elements has been suggested as a means of reconciling global heat flow predictions with observations [*Kellogg et al.*, 1999].

[34] We therefore compute the seismic properties of (1) adiabats with a range of potential temperatures and (2) nonadiabatic structures (Figure 3).

[35] Sensitivity tests indicate that S velocities are more sensitive to temperature changes than P velocities, while bulk sound and density have very small sensitivities (Figure 4). Furthermore, there is a reasonable consensus on the thermal sensitivity between different studies, where the parameter and EOS range we investigate spans published values of temperature derivatives. As a result, with increasing adiabat potential temperature, $\langle V_p \rangle$ and $\langle V_s \rangle$ decrease along a linear trend which does not intersect the global seismic data (Figure 5) because the ratio V_p/V_s of the adiabats is too high.

[36] Figure 5 also shows that with increasing potential temperature, average velocity gradients do not change

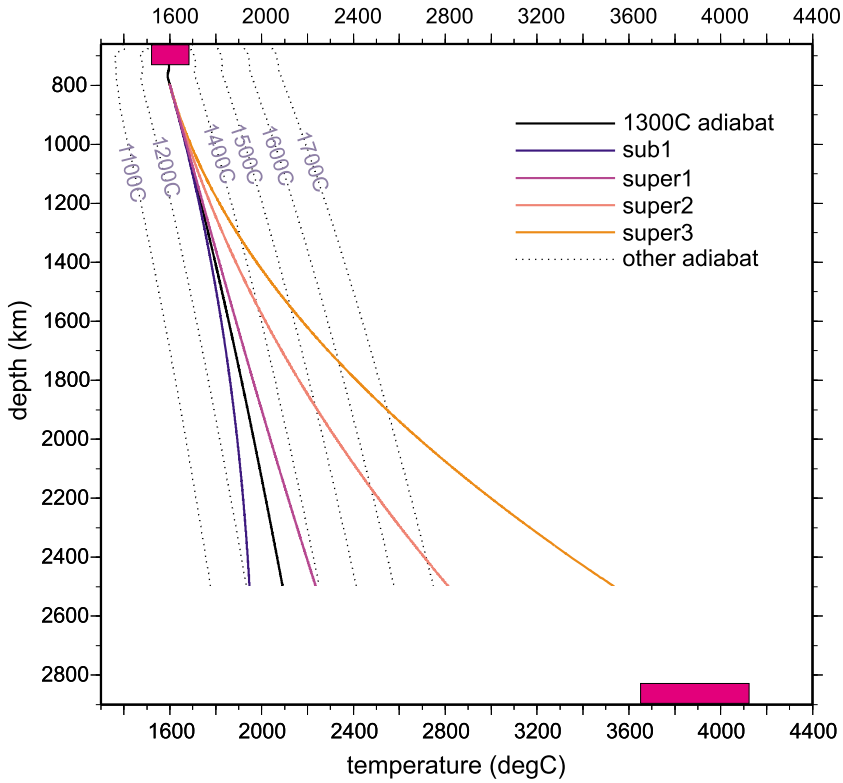

Figure 3. Illustration of the adiabatic, subadiabatic, and superadiabatic thermal structures tested in this study. The curves are labeled with the potential temperature. Pink bars show experimental constraints on lower mantle temperatures. At 660 km, the temperature of the ringwoodite to perovskite transition is inferred from high-pressure laboratory experiments [*Akaogi et al.*, 1989; *Katsura et al.*, 2004], while the maximum possible temperature at the CMB is estimated from the temperature of iron at its melting point at the inner core–outer core boundary [*Oganov et al.*, 2002].

significantly for an adiabatic structure. A nonadiabatic thermal structure is required to change the velocity gradients significantly. Subadiabats will increase gradients, and superadiabats will decrease gradients, along a linear trend (Figure 5). Therefore, a superadiabatic temperature gradient improves the fit of pyrolite to average velocity gradients below 1200 km (especially in the depth interval 1660–2000 km), but a subadiabatic gradient seems unlikely given that it reduces the fit to both average velocities and velocity gradients. This is consistent with the observation that the potential temperature of the best fitting adiabat increases with depth (Figure 5). However, a superadiabatic gradient favors absolute temperatures immediately above ~1200–1660 km which are cooler than that of a T_{pot} = 1300°C adiabat (e.g., T_{pot} ~ 1200°C); otherwise average velocities tend to become too slow below 1660 km (unless accompanied by a change in chemical composition). Figures 3 and 5 indicate that between 1660 and 2000 km a temperature excess of 50–300°C above adiabatic fits the data, which is consistent with the derivative uncertainty ranges shown in Figure 4. Note that the subadiabatic profile (Figures 3 and 5) is on average only 50°C below the adiabatic gradient in this depth interval and already does not fit the data.

4.2. Alternative Bulk Chemical Composition

4.2.1. Sensitivity Test

[37] We next examine the sensitivity of seismic velocities and density to compositional deviations from pyrolite (Figure 6). For a better insight into which aspects of chemical composition modify these properties it is necessary to consider the actual oxides from which bulk compositions are comprised, i.e., MgO, SiO_2, FeO, CaO and Al_2O_3, rather than specific "end-member" bulk compositions which may be arbitrarily defined. For each of these oxides, we have assigned a 'minimum' and 'maximum' value based on the range of molar percentages they take within proposed bulk compositions in published literature (e.g., compilations of *Poirier* [2000, and references therein] and *Williams and Knittle* [2005, and references therein]). These are 0 and 20 mol% for the minor components FeO, CaO and Al_2O_3; and 30 and 60 mol% for the major components SiO_2 and MgO. Such values are extreme (well beyond the ranges one could realistically expect for the bulk mantle) but mapping the seismic behavior of extremes is essential for understanding compositional sensitivity. In each test, we keep the relative molar ratios of four of the oxides fixed (and equal to their ratios in pyrolite), while the percentage of the remaining oxide is taken to its maximum and minimum values. Although decreases in one or other of Mg and Si are unavoidably correlated with increases in the other, we choose to study them individually for a clearer understanding of their seismic relevance.

[38] Figure 6 shows that different oxides produce markedly different seismic trends, both from each other and from the trends due to temperature changes. FeO content has a large effect on average velocities: the higher the FeO content,

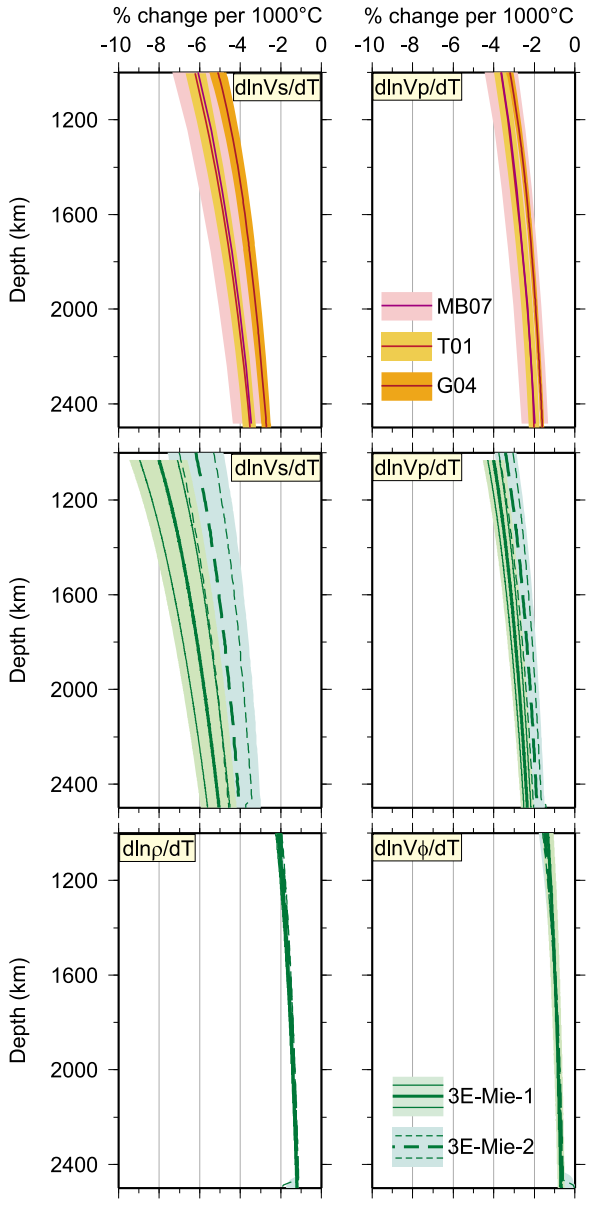

Figure 4. Temperature derivatives of V_P, V_S, bulk sound V_Φ, and density ρ, for adiabatic pyrolite. Horizontal axis shows percent change in velocity (or density) per 1000° temperature change. The 3E-Mie-1,2 are from this study. Also shown are MB07, from *Matas and Bukowinski* [2007]; T01, *Trampert et al.* [2001]; G04, *Goes et al.* [2004]. Methods 3E-Mie-1 and 3E-Mie-2 include both elastic uncertainties and anelastic uncertainties and encompass the other three published models. There is reasonably good agreement between the different studies.

the lower both V_P and V_S. Contrastingly, the higher the SiO_2 content, the higher are both V_P and V_S. SiO_2 content has a larger effect on V_S than V_P. Meanwhile, increasing the MgO content lowers V_P but has a very minor effect on V_S.

[39] The effects of Al_2O_3 and CaO are uncertain. Figure 6 implies that Al_2O_3 has a negligible effect on both V_P and V_S. However, the phase behavior of aluminum in the lower mantle is unclear. In our calculations, all Al_2O_3 is incorporated into perovskite but in reality some may partition into another Al-rich phase [*Perrillat et al.*, 2006], with different seismic properties. Nonetheless given the small volumetric significance of aluminum, the effect of an alternative phase is not expected to be major. For CaO, method 3E-Mie-2 predicts higher values of V_S without much change in V_P, but method 3E-Mie-1 suggests little seismic sensitivity to CaO changes. Previously, *Deschamps and Trampert* [2003, 2004] also found a low sensitivity of seismic velocities to calcium content, approximately an order of magnitude smaller than the sensitivity to iron content. Tighter constraints on the elastic properties of CaO would help to constrain this further.

[40] We have not included velocity gradients in Figure 6: the effect of different compositions on velocity gradients is small relative to elastic parameter uncertainties and does not improve the fit to seismic data. Composition would need to change gradually with depth from a faster to a slower material in order to reduce the velocity gradients as required between 1660 and 2000 km.

[41] Note that Fe-rich compositions lead to low bulk and shear velocities but high densities, whereas Si-rich/Mg-poor compositions lead to high bulk velocities and high densities without much change in shear velocity, at temperatures close to the 1300°C adiabat.

4.2.2. Possible Alternative Compositions

[42] We now show the seismic behavior of four bulk compositions in which we might expect the lower mantle to be enriched (Figure 7). Two of these are MORB and harzburgite, since both these compositions would appear to be seismically significant around and above the transition zone [*Cobden et al.*, 2008], and accumulated subducted material has been proposed as a source for lower mantle chemical heterogeneity [*Coltice and Ricard*, 1999]. The other two are possibilities associated with primitive material in the lower mantle.

[43] It is commonly assumed that the Earth's bulk chemical composition is given by that of the solar nebula, minus volatiles [*Poirier*, 2000]. One can therefore surmise that a close approximation to Earth's bulk composition is represented by chondritic meteorites, the oldest type of meteorite, unmodified by igneous processes, with nonvolatile elemental abundances similar to the solar photosphere [e.g., *Palme and O'Neill*, 2003]. There are several different classes of chondrite, and elemental abundances can vary by as much as 5–10% between different compilations even within the same subgroup [*Lyubetskaya and Korenaga*, 2007a]. However, in spite of these variations, and in spite of the fact that several different classes have been proposed as a representation of the Earth [e.g., *Javoy*, 1995], the majority of chondrites (ordinary, enstatite, carbonaceous) are enriched in silicon relative to pyrolite [*Williams and Knittle*, 2005]. For a chondritic bulk Earth, the "missing" silicon could be segregated somewhere within the lower mantle [*Williams and Knittle*, 2005]. If so, then seismically we might expect to detect a lower mantle composition that is closer to chondritic than pyrolitic. We therefore test the C1 chondrite composition of *Hart and Zindler* [1986] since C1 chondrites have historically been the most widely cited primitive Earth composition. Of course, it is entirely plausible that bulk primitive Earth composition is something other than chondritic [*Drake and Righter*, 2002]. *Anderson* [1989] argues that chondrite element abundances may be less similar to

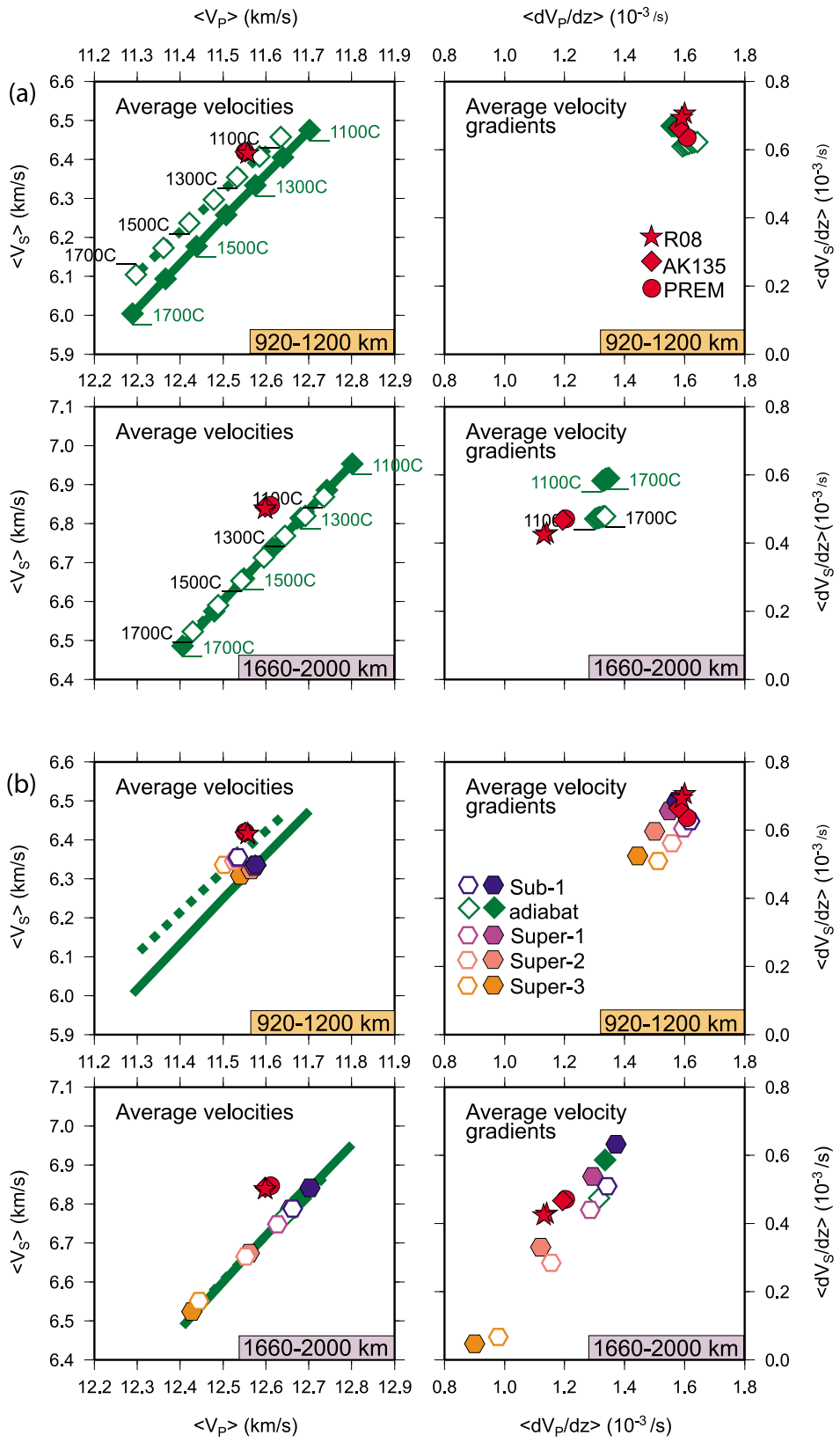

Figure 5. Average lower mantle velocities and velocity gradients for different thermal structures: (a) adiabats and (b) nonadiabats. Sub-1 and super-1, super-2, and super-3 refer to the temperature profiles illustrated in Figure 3. Solid symbols are output using method 3E-Mie-1; open symbols represent output from method 3E-Mie-2. Note that superadiabatic profiles improve the fit to average velocity gradients between 1660 and 2000 km and that the average velocities of nonadiabtic structures lie along the same trend line as the adiabatic structures.

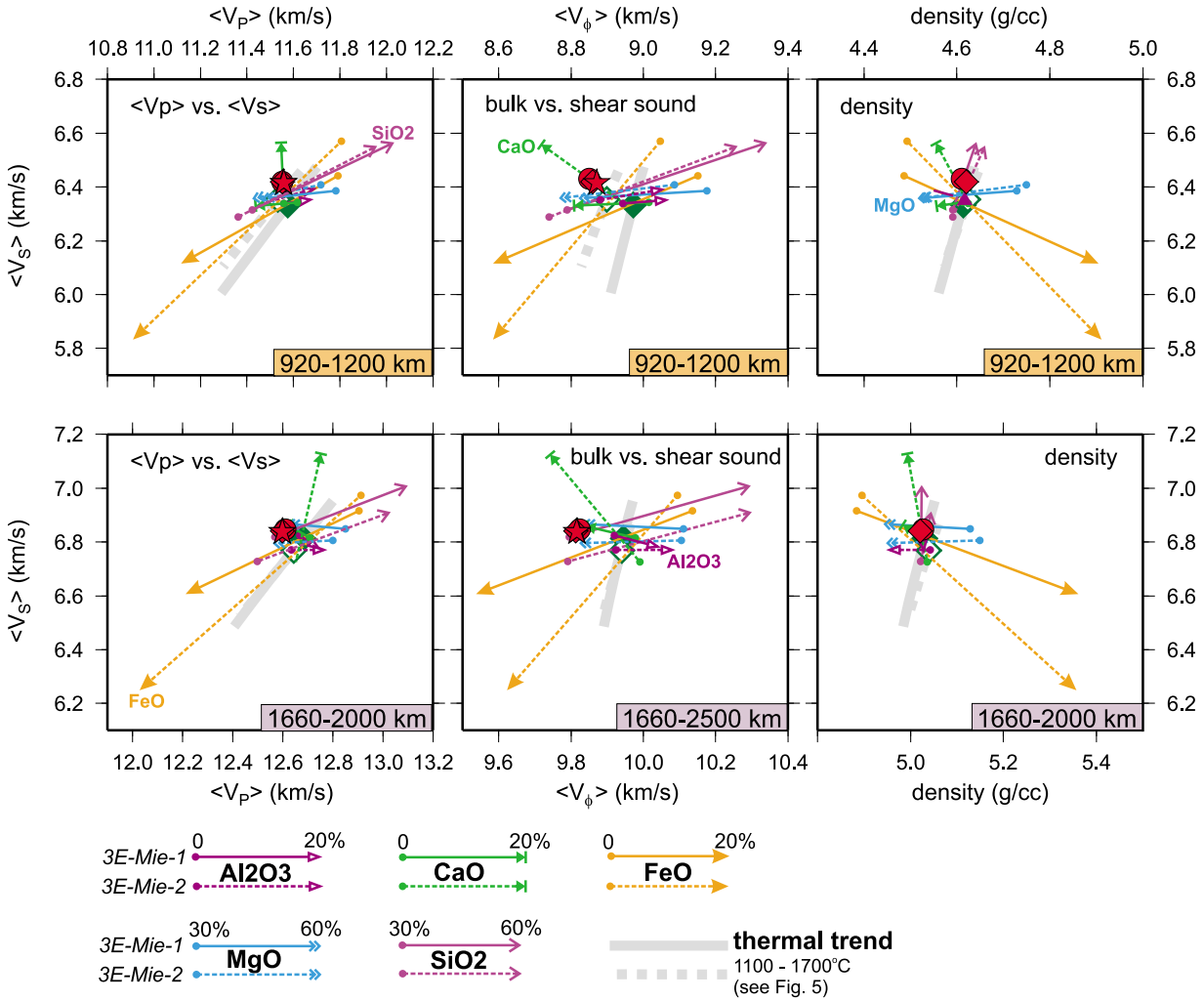

Figure 6. Velocity and density trends for changes in bulk composition, parameterized in terms of the 5 oxides Al_2O_3, CaO, FeO, MgO and SiO_2. See text for further details. Solid arrows are results using 3E-Mie-1 EOS; dashed arrows are from 3E-Mie-2. Pyrolite (green diamonds) and thermal trend (gray band, from Figure 5) are shown for comparison. Alternative compositions all computed using a Tp = 1300C adiabat for the thermal structure.

solar abundances than is often perceived, and on the basis of photospheric composition analyses, suggests an iron-rich "solar" composition as a possible alternative for bulk primitive Earth. As this composition is quite distinct from the others we test (Table 1) it has been included in this study.

[44] Figure 7 shows that no single composition can improve the fit to the seismic data. At all depth intervals, MORB has the highest average P and S velocities (a consequence of its having a low MgO and high SiO_2 content) (Table 1). The seismic properties of harzburgite and chondrite likewise are predominantly controlled by their Mg/Si ratio, with chondrite lying intermediate between pyrolite and MORB, and harzburgite very similar to pyrolite. However, the seismic behavior of the solar composition is dominated by its high iron content: even though it has a relatively low MgO content which would tend to increase P velocities, it attains the lowest P velocities overall due to the stronger effect of iron. This is interesting because it implies that it is important to consider both variations in Mg/Si ratio and variations in Fe content when attempting either to model or interpret data for the lower mantle.

[45] Tests with alternative MORB compositions which attempt to correct for the absence of Na from our calculations indicate that MORB is always characterized by elevated V_P, but its V_S may increase or decrease relative to pyrolite, for a T_P = 1300°C adiabat. At high temperatures, all MORB compositions tested show a reduction in V_S.

5. Discussion: Adiabatic Pyrolite or Something Else?

[46] Our results indicate that adiabatic pyrolite is unlikely to be the most suitable average thermochemical model for the lower mantle, but cannot be ruled out completely at this stage, given the current uncertainties in the elastic parameters. In particular, it is difficult to fit velocity gradients, and to a lesser extent velocities, below 1660 km, using an adiabatic temperature gradient. Our sensitivity tests suggest

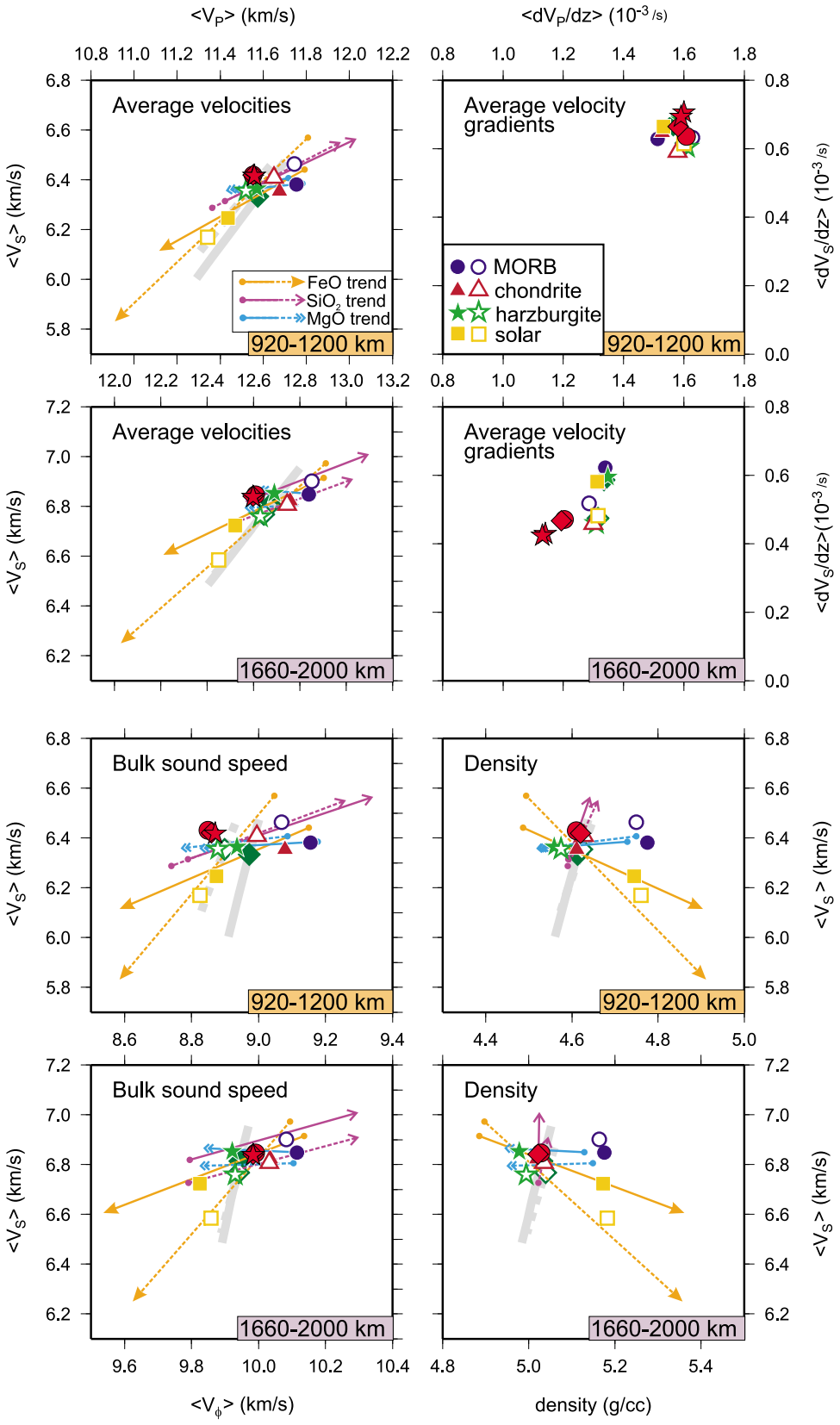

Figure 7. Average velocities, velocity gradients, and densities for different bulk compositions (defined in Table 1) in which the lower mantle may be enriched. Solid symbols and lines were calculated using method 3E-Mie-1; open symbols and dashed lines were calculated using method 3E-Mie-2. Red data points are seismic constraints. Alternative compositions all computed using a Tp = 1300°C adiabat for the thermal structure. Grey bars show change in properties with temperature from Figure 5.

Table 1. End-Member Compositions Tested in This Study[a]

	SiO_2	MgO	Al_2O_3	FeO	CaO	Mg/Si	Source
Pyrolite	38.61	49.13	2.77	6.24	3.25	1.272468	*Sun* [1982]
Harzburgite	36.22	57.42	0.48	5.44	0.44	1.585312	*Irifune and Ringwood* [1987]
MORB	53.82	13.64	10.13	8.80	13.60	0.253437	*Perrillat et al.* [2006]
Chondrite	43.52	46.74	1.84	5.25	2.66	1.074112	*Hart and Zindler* [1986]
Solar	40.03	43.37	1.68	11.68	3.24	1.083306	*Anderson* [1989]

[a]Compositions are expressed as molar percentages.

several possible ways of obtaining a better fit to the seismic data than adiabatic pyrolite.

5.1. Purely Thermally

[47] It is possible to devise a thermal structure which will completely fit the 1-D seismic data used in this study. Such a structure would require a superadiabatic gradient incipient at some point below 1200 km, and especially marked between 1660 and 2000 km (~0.4 to 0.8°C per km), together with an initial surface potential temperature at 800 km of ~1200°C (Figure 5). However, other studies indicate that while a superadiabatic gradient is likely at these depths [*da Silva et al.*, 2000; *Khan et al.*, 2008; *Verhoeven et al.*, 2009], it is difficult to invoke superadiabaticity as a mechanism to fit all other lower mantle observations. First, the density of warm (superadiabatic) pyrolite is too low relative to PREM in the lowermost mantle [*Aizawa and Yoneda*, 2006; *Lee et al.*, 2004]: a concurrent chemical change would be needed to increase density. Second, as discussed in section 1, geochemistry requires there to be some chemical heterogeneity at depth. It is been suggested that such heterogeneity may only be present on very small scales such that the majority of the mantle has a uniform (MORB source) composition [*Lyubetskaya and Korenaga*, 2007b]. However, this leads to difficulty in explaining the seismic characteristics of the Pacific and African superplumes, which are now widely accepted as chemically distinct domains [e.g., *Trampert et al.*, 2004; *Ishii and Tromp*, 1999]. If such large regions are indeed chemically distinct from the surrounding mantle, one would expect the 1-D average seismic structure to be influenced by them, as is the case for the upper mantle [e.g., *Cobden et al.*, 2008], unless either the seismic sum of the "superplume" domains and nonsuperplume domains coincidentally averages out to that of pyrolite, or the mineral physics uncertainties are larger than the shifts in 1-D average velocity which occur due to compositional variations.

[48] It is worth considering also the effect of iron spin transitions. Experiments indicate a transition from high to low spin state in iron in ferropericlase somewhere between 40 and 90 GPa (~1100–2100 km) depending on iron content [*Speziale et al.*, 2007] and that low-spin ferropericlase is associated with higher densities and velocities than its high-spin counterpart [*Lin et al.*, 2006]. *Badro et al.* [2005] suggest that thermal conductivity may be enhanced in low-spin FeO. This could result in superadiabaticity in the lowermost mantle, at higher densities than are predicted for high-spin FeO. However, the most recent experiments on the spin transition [*Crowhurst et al.*, 2008] indicate that during the broad depth interval over which the transition takes place (~40–60 GPa), there is a transient softening of the elastic moduli, with a reduction in *P* and *S* velocities. As ferropericlase is globally ubiquitous in the lower mantle, a signal of this softening ought to be detectable in 1-D radial seismic profiles. However, the 1-D seismic velocities increase smoothly and continuously with depth (Figure 1), so the actual existence of such a transition in the lower mantle, or how it can be reconciled with the seismic data, remains uncertain.

5.2. Chemically (Plus/Minus Thermal Component)

[49] There are two dominant controls on seismic velocities: FeO, which causes reduced *P* and *S* velocities with increasing iron content, and Mg/Si ratio, which leads to higher *P* and *S* velocities as the ratio decreases, although with a stronger effect in *P* (Figure 6). From a first glance at the velocity profiles in Figure 8, the most striking observation is that an iron-rich composition (represented here by *Anderson*'s [1989] solar composition) would appear to provide a better fit to both *P* and *S* velocities below ~2250 km depth than any of the other compositions, and indeed this may be the case for the Earth's lower mantle (potentially through having a composition with a solar component). However, pyrolite starts to deviate from the seismic references several hundred km above this depth (Figure 2), so thermochemical changes are also required above this depth. If the high velocity gradients of pyrolite between 1660 and 2000 km are to be reduced purely compositionally, then this requires a gradual shift to a seismically slower composition with increasing depth. Either Fe enrichment or increasing the Mg/Si ratio could be invoked.

[50] The problem with Fe enrichment is that if it starts to happen as shallow as 1660 km, then average velocities become too slow (Figure 6), unless the lower mantle is relatively cold. Additionally, the high density of iron may cause Fe-enriched material to stagnate, thereby reducing convective overturn, which would in turn increase temperature gradients (i.e., superadiabaticity). Such superadiabaticity would cause the velocities to be even slower.

[51] Several other studies have concluded that an increase in Mg content is needed to fit various seismic and gravity constraints [*Aizawa and Yoneda*, 2006; *Khan et al.*, 2008; *Lee et al.*, 2004], i.e., an increase in Mg/Si ratio. However, the problem with increasing the Mg/Si ratio is that it may not produce sufficiently strong reductions in *S* velocities, which would seem to be required to fit the 1-D average gradients, once mineral physics uncertainties are taken into account (Figure 2). Furthermore, it is difficult to provide a physical explanation for the high Mg/Si ratio, as both MORBs and chondrites (compositions in which one might expect the lower mantle to be enriched) are characterized by low Mg/Si ratios (Table 1).

[52] Another candidate to consider is Si enrichment/Mg depletion (as associated with enrichment in MORB or a chondritic composition). For a 1300°C adiabat, high Si/Mg

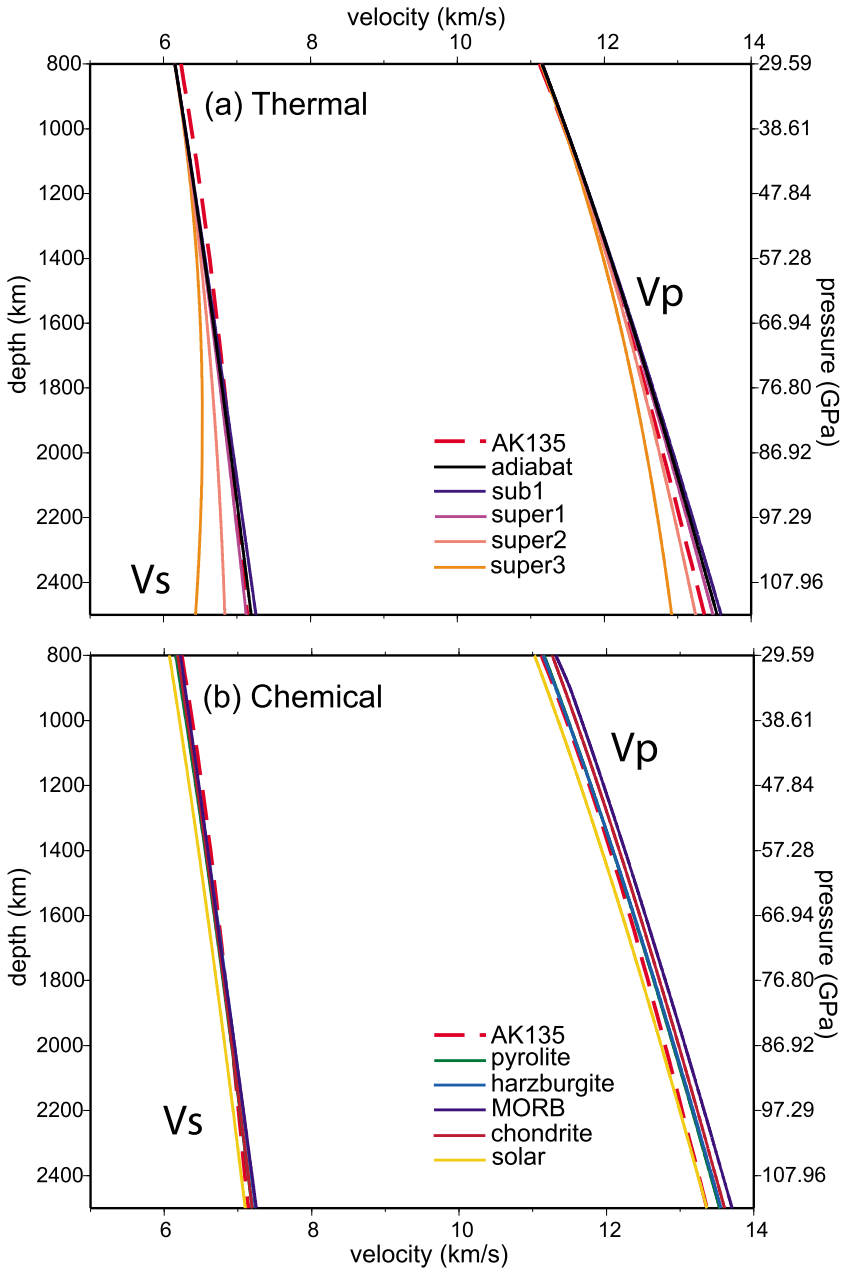

Figure 8. Velocity-depth profiles for alternative (a) thermal and (b) chemical structures tested in this study. Note that superadiabatic structures reduce gradients, providing a means of improving fit to the seismic data. Compositionally, note the fit of the solar (i.e., iron-enriched) composition in the lowermost mantle.

compositions such as MORB and chondrite increase *P* velocities relative to pyrolite, such as to pull a pyrolite-based composition further away from the seismic data. This is the case even taking elastic parameter uncertainties into account. At higher temperatures, as would occur with a superadiabatic gradient, *P* velocities are reduced along the thermal trend indicated in Figure 7. With our MORB composition (Table 1), then at present the equation of state we used, together with the elastic parameter uncertainties, still preclude hot MORB from fitting the average *P* velocities, because they are still too high. However, a composition with a slightly less elevated Si/Mg ratio could potentially fit the *P* velocities.

[53] Therefore, we suggest that superadiabatic basalt may be a volumetrically significant component in the lowermost mantle because it has a number of physical properties consistent with LLSVPs, namely, a high density and high bulk sound velocities, with low shear velocities (Figure 7). Analyses of global geodynamic data [*Forte and Mitrovica*, 2001] and numerical modeling of mantle convection [*Tan and Gurnis*, 2007] have yielded similar conclusions. The fact that superadiabatic basalt does not reconcile all seismic constraints simultaneously, and that no other thermo-chemical structure does either, is indicative that further work is required in refining the equation of state, and associated mineral elastic parameters, for the lower mantle,

together with tighter constraints on the phase relations in MORB-like compositions. Equally, it shows that we need to consider how 3-D thermochemical variations can detectably map into the one-dimensional seismic average. Such biases in reference structure would affect interpretation of seismic anomalies of the deep mantle.

Appendix A: Reversible Jump Markov Chain Monte Carlo Algorithm

A1. Procedure

[54] We use a recently developed statistical method of sampling, the reversible jump Markov chain Monte Carlo (RJMCMC) algorithm, to invert *P* and *S* teleseismic travel times for the 1-D velocity structure of the lower mantle. The RJMCMC method was established by P. J. Green [*Green*, 1995, 2001, 2003] and recent reviews have been given by *Sambridge et al.* [2006] and *Gallagher et al.* [2009]. The most important feature of RJMCMC is that it allows jumps between models of different dimensions during inversion. That is, the number of model parameters varies during the inversion and is itself treated as an unknown parameter to be solved for. This method is extremely suited to solving the travel time inversion problem, because it avoids the need for an a priori segmentation of the Earth into a fixed number of layers, and allows us to investigate the required smoothness of the velocity profile.

[55] The RJMCMC algorithm is designed to generate a Markov chain, i.e., a sequence of models (converging to the solution space) in which the values of the parameters of the updated model depend only on the values of the parameters of the previous model. At each stage in the chain, an ''acceptance probability'' α for the proposed model is calculated. If $\vec{x}$ and $\vec{x}'$ are the model parameter vectors of the current and proposed model, then, according to *Green* [1995], α is given by

$$\alpha(\vec{x},\vec{x}') = \frac{\pi(\vec{x}')q(\vec{x},\vec{x}')}{\pi(\vec{x})q(\vec{x}',\vec{x})} JR|J| \tag{A1}$$

where $\pi(\vec{x})$ is the target distribution in the model space, which approximates to the solution space; $q(\vec{x}, \vec{x}')$ is the proposal probability density function, which is used to perturb the model parameters; *JR* is the jump ratio, or the ratio of the probability of proposing the proposed move to the probability of proposing the reverse move, and $|J|$ is the Jacobian of the transformation.

[56] If Bayesian inference is used, as in our case, then $\pi(\vec{x})$ is seen is a posterior probability distribution of the model parameters $\vec{x}$, conditional on the observed data d_{obs}, and according to Bayes' theorem,

$$\pi(\vec{x}) \propto L(d_{obs}|\vec{x})p(\vec{x}) \tag{A2}$$

where $L(d_{obs}|\vec{x})$ is a likelihood function calculated from the observed seismic data for the model $\vec{x}$, and $p(\vec{x})$ is the prior probability distribution of the model parameters (based on prior knowledge). Substituting (A2) into (A1), we obtain

$$\alpha(\vec{x},\vec{x}') = \frac{L(d_{obs}|\vec{x}')p(\vec{x}')q(\vec{x},\vec{x}')}{L(d_{obs}|\vec{x})p(\vec{x})q(\vec{x}',\vec{x})} JR|J| \tag{A3}$$

The proposed model is accepted if a random number between 0 and 1, drawn from a uniform distribution, is less than $\alpha(\vec{x}, \vec{x}')$. If accepted, the proposed model $\vec{x}'$ becomes $\vec{x}$ during the next step of the chain.

A2. Data Input

[57] Travel time data are taken from the ISC catalog reprocessed by *Engdahl et al.* [1998] (also E. R. Engdahl, personal communication, 2000). We consider direct *P* and *S* arrivals only, in the epicentral distance ranges 24.75–89.75° and 23.25–79.75° respectively. We compute mean travel times as a function of epicentral distance at 0.5° intervals and assume an uncertainty on these times equal to 3 times the standard deviation of the mean. We find that the uncertainty is approximately constant with epicentral distance for both *P* and *S* waves, at ±0.15 s for *P* and ±1 s for *S*.

[58] The likelihood function $L(d_{obs}|\vec{x})$ required to quantify the misfit between simulated and observed data (equation (A3)), is given by

$$L\left(\overrightarrow{tt}_{obs}|\vec{x}\right) = \frac{1}{\left[(2\pi)^N \det(E)\right]^{1/2}} \exp\left(-\frac{1}{2}\left(\overrightarrow{tt}_{obs} - \overrightarrow{tt}_{pred}(\vec{x})\right)^T \cdot E^{-1}\left(\overrightarrow{tt}_{obs} - \overrightarrow{tt}_{pred}(\vec{x})\right)\right) \tag{A4}$$

where we have assumed that the measurement errors for travel times have a normal distribution with zero mean and are uncorrelated; $(\overrightarrow{tt}_{obs} - \overrightarrow{tt}_{pred}(\vec{x}))$ is the difference between the observed travel times and those predicted by the model parameters $\vec{x}$; *E* is the covariance matrix of the measurement error vector, and N is the number of measurements (i.e., number of epicentral distances at which mean travel times are calculated). With the assumption of uncorrelated measurement errors, *E* is diagonal, and the exponential component of equation (A4) can be written as

$$-0.5 * \sum_{i=1}^{N} \left(\frac{\overrightarrow{tt}_{obs_i} - \overrightarrow{tt}_{pred_i}(\vec{x})}{\sigma_i}\right)^2$$

where σ_i is the uncertainty on the *i*th mean travel time, taken to be constant over the whole epicentral distance range (see above). This expression is also referred to as the log likelihood (minus a constant term).

[59] The synthetic model $\vec{x}$ has three components: a number of layers, depths of the layer interfaces, and velocities at each interface. We set the prior function $p(\vec{x})$ for each of these parameters to a uniform distribution, i.e., every value within a defined range is as likely as any other. For example, with the velocities, the prior distribution is centered around the AK135 mean value, with a range of ±1 km/s. For number of layers, the distribution ranges uniformly from 2 to 50 layers. Interface depths span the depth range of the lower mantle (660 to 2891 km). Details of the proposal distributions, $q(\vec{x}, \vec{x}')$, are beyond the scope of this paper, and for further information the reader is referred to *Ravenna* [2009].

[60] **Acknowledgments.** We are grateful to Ian Jackson and an anonymous reviewer whose comments helped to improve the manuscript. We thank Lars Stixrude for assistance with implementing their databases into Perple_X, and Paul Tackley for providing output from his dynamic thermochemical models for comparison with our interpretations.

References

Aizawa, Y., and A. Yoneda (2006), P-V-T equation of state of $MgSiO_3$ perovskite and MgO periclase: Implication for lower mantle composition, *Phys. Earth Planet. Inter.*, *155*, 87–95, doi:10.1016/j.pepi.2005.10.002.

Akaogi, M., et al. (1989), Olivine-modified spinel-spinel transitions in the system Mg_2SiO_4-Fe_2SiO_4: Calorimetric measurements, thermochemical calculation, and geophysical application, *J. Geophys. Res.*, *94*, 15,671–15,685, doi:10.1029/JB094iB11p15671.

Albarede, F., and R. D. van der Hilst (2002), Zoned mantle convection, *Philos. Trans. R. Soc. London, Ser. A*, *360*, 2569–2592, doi:10.1098/rsta.2002.1081.

Anderson, D. L. (1989), Composition of the Earth, *Science*, *243*, 367–370, doi:10.1126/science.243.4889.367.

Anderson, D. L. (2007), *New Theory of the Earth*, 1st ed., 384 pp., Cambridge Univ. Press, Cambridge, U. K.

Anderson, O. L., et al. (1995), A new thermodynamic approach for high-pressure physics, *Phys. Earth Planet. Inter.*, *91*, 3–16, doi:10.1016/0031-9201(95)03044-W.

Badro, J., et al. (2003), Iron partitioning in Earth's mantle: Toward a deep lower mantle discontinuity, *Science*, *300*, 789–791, doi:10.1126/science.1081311.

Badro, J., et al. (2005), Thermochemical state of the lower mantle: New insights from mineral physics, in *Earth's Deep Mantle: Structure, Composition and Evolution*, *Geophys. Monogr. Ser.*, vol. 160, edited by R. Van der Hilst et al., pp. 241–260, AGU, Washington, D. C.

Birch, F. (1952), Elasticity and constitution of the Earth's interior, *J. Geophys. Res.*, *57*, 227–286, doi:10.1029/JZ057i002p00227.

Brodholt, J. P., et al. (2007), Chemical versus thermal heterogeneity in the lower mantle: The most likely role of anelasticity, *Earth Planet. Sci. Lett.*, *262*, 429–437, doi:10.1016/j.epsl.2007.07.054.

Bunge, H. P., et al. (2001), Non-adiabaticity in mantle convection, *Geophys. Res. Lett.*, *28*, 879–882, doi:10.1029/2000GL011864.

Cammarano, F., et al. (2003), Inferring upper-mantle temperatures from seismic velocities, *Phys. Earth Planet. Inter.*, *138*, 197–222, doi:10.1016/S0031-9201(03)00156-0.

Cammarano, F., et al. (2005a), One dimensional physical reference models for the upper mantle and transition zone: Combining seismic and mineral physics constraints, *J. Geophys. Res.*, *110*, B01306, doi:10.1029/2004JB003272.

Cammarano, F., et al. (2005b), Is a pyrolitic mantle compatible with seismic data?, *Earth Planet. Sci. Lett.*, *232*, 227–243, doi:10.1016/j.epsl.2005.01.031.

Cobden, L., et al. (2008), Thermochemical interpretation of one-dimensional seismic reference models for the upper mantle: Evidence for bias due to heterogeneity, *Geophys. J. Int.*, *175*, 627–648, doi:10.1111/j.1365-246X.2008.03903.x.

Coltice, N., and Y. Ricard (1999), Geochemical observations and one layer mantle convection, *Earth Planet. Sci. Lett.*, *174*, 125–137, doi:10.1016/S0012-821X(99)00258-7.

Connolly, J. A. D. (1990), Multivariable phase diagrams—An algorithm based on generalized thermodynamics, *Am. J. Sci.*, *290*, 666–718.

Connolly, J. A. D. (2005), Computation of phase equilibria by linear programming: A tool for geodynamic modeling and its application to subduction zone decarbonation, *Earth Planet. Sci. Lett.*, *236*, 524–541, doi:10.1016/j.epsl.2005.04.033.

Crotwell, H. P., et al. (1999), The TauP Toolkit: Flexible travel time and ray path utilities, *Seismol. Res. Lett.*, *70*, 154–160.

Crowhurst, J. C., et al. (2008), Elasticity of (Mg, Fe)O through the spin transition of iron in the lower mantle, *Science*, *319*, 451–453, doi:10.1126/science.1149606.

da Silva, C. R. S., et al. (2000), The composition and geotherm of the lower mantle: Constraints from the elasticity of silicate perovskite, *Phys. Earth Planet. Inter.*, *118*, 103–109, doi:10.1016/S0031-9201(99)00133-8.

Davies, G. F., and A. M. Dziewonski (1975), Homogeneity and constitution of Earth's lower mantle and outer core, *Phys. Earth Planet. Inter.*, *10*, 336–343, doi:10.1016/0031-9201(75)90060-6.

Deschamps, F., and J. Trampert (2003), Mantle tomography and its relation to temperature and composition, *Phys. Earth Planet. Inter.*, *140*, 277–291, doi:10.1016/j.pepi.2003.09.004.

Deschamps, F., and J. Trampert (2004), Towards a lower mantle reference temperature and composition, *Earth Planet. Sci. Lett.*, *222*, 161–175, doi:10.1016/j.epsl.2004.02.024.

Drake, M. J., and K. Righter (2002), Determining the composition of the Earth, *Nature*, *416*, 39–44, doi:10.1038/416039a.

Dziewonski, A. M., and D. L. Anderson (1981), Preliminary reference Earth model, *Phys. Earth Planet. Inter.*, *25*, 297–356, doi:10.1016/0031-9201(81)90046-7.

Engdahl, E. R., R. Van der Hilst, and R. Buland (1998), Global teleseismic earthquake relocation with improved travel times and procedures for depth determination, *Bull. Seismol. Soc. Am.*, *88*, 722–743.

Forte, A. M., and J. X. Mitrovica (2001), Deep-mantle high-viscosity flow and thermochemical structure inferred from seismic and geodynamic data, *Nature*, *410*, 1049–1056, doi:10.1038/35074000.

Gallagher, K., et al. (2009), Markov chain Monte Carlo (MCMC) sampling methods to determine optimal models, model resolution and model choice for Earth science problems, *Mar. Pet. Geol.*, *26*, 525–535, doi:10.1016/j.marpetgeo.2009.01.003.

Goes, S., et al. (2004), Synthetic seismic signature of thermal mantle plumes, *Earth Planet. Sci. Lett.*, *218*, 403–419, doi:10.1016/S0012-821X(03)00680-0.

Grand, S. P., et al. (1997), High resolution global tomography: A snapshot of convection in the Earth, *GSA Today*, *7*, 1–7.

Green, P. J. (1995), Reversible jump Markov chain Monte Carlo computation and Bayesian model determination, *Biometrika*, *82*, 711–732, doi:10.1093/biomet/82.4.711.

Green, P. J. (2001), A primer on Markov chain Monte Carlo, in *Highly Structured Stochastic Systems*, *Oxford Stat. Sci. Ser.*, vol. 27, edited by O. L. Barndorff-Nielsen et al., pp. 179–196, Oxford Univ. Press, Oxford, U. K.

Green, P. J. (2003), Trans-dimensional MCMC, in *Highly Structured Stochastic Systems*, *Oxford Stat. Sci. Ser.*, vol. 27, edited by O. L. Barndorff-Nielsen et al., pp. 179–196, Oxford Univ. Press, Oxford, U. K.

Hart, S. R., and A. Zindler (1986), In search of a bulk-earth composition, *Chem. Geol.*, *57*, 247–267, doi:10.1016/0009-2541(86)90053-7.

Hofmann, A. W. (1997), Mantle geochemistry: The message from oceanic volcanism, *Nature*, *385*, 219–229, doi:10.1038/385219a0.

Irifune, T., and A. E. Ringwood (1987), Phase-transformations in a harzburgite composition to 26 GPa—Implications for dynamical behavior of the subducting slab, *Earth Planet. Sci. Lett.*, *86*, 365–376, doi:10.1016/0012-821X(87)90233-0.

Ishii, M., and J. Tromp (1999), Normal-mode and free-air gravity constraints on lateral variations in velocity and density of Earth's mantle, *Science*, *285*, 1231–1236, doi:10.1126/science.285.5431.1231.

Jackson, I. (1998), Elasticity, composition and temperature of the Earth's lower mantle: A reappraisal, *Geophys. J. Int.*, *134*, 291–311, doi:10.1046/j.1365-246x.1998.00560.x.

Jackson, J. M., S. V. Sinogeikin, S. D. Jacobsen, H. J. Reichmann, S. J. Mackwell, and J. D. Bass (2006), Single-crystal elasticity and sound velocities of $(Mg_{0.94}Fe_{0.06})O$ ferropericlase to 20 GPa, *J. Geophys. Res.*, *111*, B09203, doi:10.1029/2005JB004052.

Javoy, M. (1995), The integral enstatite chondrite model of the Earth, *Geophys. Res. Lett.*, *22*, 2219–2222, doi:10.1029/95GL02015.

Jeffreys, H., and K. E. Bullen (1940), *Seismological Tables*, Br. Assoc. Seismol. Comm., London.

Karato, S. (1993), Importance of Anelasticity in the Interpretation of Seismic Tomography, *Geophys. Res. Lett.*, *20*, 1623–1626, doi:10.1029/93GL01767.

Katsura, T., et al. (2004), Olivine-wadsleyite transition in the system $(Mg, Fe)_2SiO_4$, *J. Geophys. Res.*, *109*, B02209, doi:10.1029/2003JB002438.

Kellogg, L. H., et al. (1999), Compositional stratification in the deep mantle, *Science*, *283*, 1881–1884, doi:10.1126/science.283.5409.1881.

Kennett, B. L. N., et al. (1995), Constraints on seismic velocities in the Earth from traveltimes, *Geophys. J. Int.*, *122*, 108–124, doi:10.1111/j.1365-246X.1995.tb03540.x.

Kennett, B. L. N., et al. (1998), Joint seismic tomography for bulk sound and shear wave speed in the Earth's mantle, *J. Geophys. Res.*, *103*, 12,469–12,493, doi:10.1029/98JB00150.

Khan, A., J. A. D. Connolly, and N. Olsen (2006), Constraining the composition and thermal state of the mantle beneath Europe from inversion of long-period electromagnetic sounding data, *J. Geophys. Res.*, *111*, B10102, doi:10.1029/2006JB004270.

Khan, A., J. A. D. Connolly, and S. R. Taylor (2008), Inversion of seismic and geodetic data for the major element chemistry and temperature of the Earth's mantle, *J. Geophys. Res.*, *113*, B09308, doi:10.1029/2007JB005239.

Lee, K. K. M., et al. (2004), Equations of state of the high-pressure phases of a natural peridotite and implications for the Earth's lower mantle, *Earth Planet. Sci. Lett.*, *223*, 381–393, doi:10.1016/j.epsl.2004.04.033.

Li, B. S., and J. Z. Zhang (2005), Pressure and temperature dependence of elastic wave velocity of $MgSiO_3$ perovskite and the composition of the lower, *Phys. Earth Planet. Inter.*, *151*, 143–154.

Lin, J.-F., S. D. Jacobsen, W. Sturhahn, J. M. Jackson, J. Zhao, and C.-S. Yoo (2006), Sound velocities of ferropericlase in the Earth's lower mantle, *Geophys. Res. Lett.*, *33*, L22304, doi:10.1029/2006GL028099.

Lyubetskaya, T., and J. Korenaga (2007a), Chemical composition of Earth's primitive mantle and its variance: 1. Method and results, *J. Geophys. Res.*, *112*, B03211, doi:10.1029/2005JB004223.

Lyubetskaya, T., and J. Korenaga (2007b), Chemical composition of Earth's primitive mantle and its variance: 2. Implications for global geodynamics, *J. Geophys. Res.*, *112*, B03212, doi:10.1029/2005JB004224.

Masters, G., et al. (2000), The relative behaviour of shear velocity, bulk sound speed, and compressional velocity in the mantle: Implications for chemical and thermal structure, in *Earth's Deep Interior: Mineral Physics and Tomography From the Atomic to the Global Scale*, *Geophys. Monogr. Ser.*, vol. 117, edited by S. I. Karato et al., pp. 63–87, AGU, Washington, D. C.

Matas, J., and M. S. T. Bukowinski (2007), On the anelastic contribution to the temperature dependence of lower mantle seismic velocities, *Earth Planet. Sci. Lett.*, *259*, 51–65, doi:10.1016/j.epsl.2007.04.028.

Matas, J., et al. (2007), On the bulk composition of the lower mantle: Predictions and limitations from generalized inversion of radial seismic profiles, *Geophys. J. Int.*, *170*, 764–780, doi:10.1111/j.1365-246X.2007.03454.x.

Mattern, E., et al. (2005), Lower mantle composition and temperature from mineral physics and thermodynamic modelling, *Geophys. J. Int.*, *160*, 973–990, doi:10.1111/j.1365-246X.2004.02549.x.

Nakagawa, T., and P. J. Tackley (2004), Thermo-chemical structure in the mantle arising from a three-component convective system and implications for geochemistry, *Phys. Earth Planet. Inter.*, *146*, 125–138, doi:10.1016/j.pepi.2003.05.006.

Oganov, A. R., et al. (2002), Ab initio theory of phase transitions and thermoelasticity of minerals, *EMU Notes in Mineralogy*, vol. 4, *Energy Modelling in Minerals*, edited by C. M. Gramaccioli, pp. 83–170, Eur. Mineral. Union, Vienna.

Ohta, K., et al. (2008), Phase transitions in pyrolite and MORB at lowermost mantle conditions: Implications for a MORB-rich pile above the core-mantle boundary, *Earth Planet. Sci. Lett.*, *267*, 107–117, doi:10.1016/j.epsl.2007.11.037.

Palme, H., and B. O'Neill (2003), Cosmochemical estimates of mantle composition, in *Treatise in Geology*, vol. 2, *The Mantle and Core*, edited by H. Holland and K. K. Turekian, pp. 1–38, doi:10.1016/B0-08-043751-6/02177-0, Elsevier, New York.

Perrillat, J. P., et al. (2006), Phase transformations of subducted basaltic crust in the uppermost lower mantle, *Phys. Earth Planet. Inter.*, *157*, 139–149, doi:10.1016/j.pepi.2006.04.001.

Poirier, J. P. (2000), *Introduction to the Physics of the Earth's Interior*, Cambridge Univ. Press, Cambridge, U. K.

Rapp, R. P., et al. (2008), Subduction recycling of continental sediments and the origin of geochemically enriched reservoirs in the deep mantle, *Earth Planet. Sci. Lett.*, *271*, 14–23, doi:10.1016/j.epsl.2008.02.028.

Ravenna, M. (2009), A Reversible Jump Markov Chain Monte Carlo inversion method for layering and amplitude of seismic velocity variations: An application to 1-D structure of the lower mantle, Ph.D. thesis, Imp. Coll. London, London.

Resovsky, J., and J. Trampert (2003), Using probabilistic seismic tomography to test mantle velocity-density relationships, *Earth Planet. Sci. Lett.*, *215*, 121–134, doi:10.1016/S0012-821X(03)00436-9.

Saltzer, R. L., et al. (2001), Comparing P and S wave heterogeneity in the mantle, *Geophys. Res. Lett.*, *28*, 1335–1338, doi:10.1029/2000GL012339.

Sambridge, M., et al. (2006), Trans-dimensional inverse problems, model comparison and the evidence, *Geophys. J. Int.*, *167*, 528–542, doi:10.1111/j.1365-246X.2006.03155.x.

Sinha, G., and S. L. Butler (2007), On the origin and significance of subadiabatic temperature gradients in the mantle, *J. Geophys. Res.*, *112*, B10406, doi:10.1029/2006JB004850.

Speziale, S., V. E. Lee, S. M. Clark, J. F. Lin, M. P. Pasternak, and R. Jeanloz (2007), Effects of Fe spin transition on the elasticity of (Mg, Fe)O magnesiowüstites and implications for the seismological properties of the Earth's lower mantle, *J. Geophys. Res.*, *112*, B10212, doi:10.1029/2006JB004730.

Stixrude, L., and C. Lithgow-Bertelloni (2005a), Mineralogy and elasticity of the oceanic upper mantle: Origin of the low-velocity zone, *J. Geophys. Res.*, *110*, B03204, doi:10.1029/2004JB002965.

Stixrude, L., and C. Lithgow-Bertelloni (2005b), Thermodynamics of mantle minerals- I. Physical properties, *Geophys. J. Int.*, *162*, 610–632, doi:10.1111/j.1365-246X.2005.02642.x.

Stixrude, L., and C. Lithgow-Bertelloni (2007), Influence of phase transformations on lateral heterogeneity and dynamics in Earth's mantle, *Earth Planet. Sci. Lett.*, *263*, 45–55, doi:10.1016/j.epsl.2007.08.027.

Su, W. J., and A. M. Dziewonski (1997), Simultaneous inversion for 3-D variations in shear and bulk velocity in the mantle, *Phys. Earth Planet. Inter.*, *100*, 135–156, doi:10.1016/S0031-9201(96)03236-0.

Sun, S. S. (1982), Chemical-composition and origin of the Earth's primitive mantle, *Geochim. Cosmochim. Acta*, *46*, 179–192, doi:10.1016/0016-7037(82)90245-9.

Tan, E., and M. Gurnis (2007), Compressible thermochemical convection and application to lower mantle structures, *J. Geophys. Res.*, *112*, B06304, doi:10.1029/2006JB004505.

Trampert, J., et al. (2001), Sensitivities of seismic velocities to temperature, pressure and composition in the lower mantle, *Phys. Earth Planet. Inter.*, *124*, 255–267, doi:10.1016/S0031-9201(01)00201-1.

Trampert, J., et al. (2004), Probabilistic tomography maps chemical heterogeneities throughout the lower mantle, *Science*, *306*, 853–856, doi:10.1126/science.1101996.

Trieloff, M., et al. (2000), The nature of pristine noble gases in mantle plumes, *Science*, *288*, 1036–1038, doi:10.1126/science.288.5468.1036.

van der Hilst, R. D., and H. Karason (1999), Compositional heterogeneity in the bottom 1000 kilometers of Earth's mantle: Toward a hybrid convection model, *Science*, *283*, 1885–1888, doi:10.1126/science.283.5409.1885.

van der Hilst, R. D., et al. (1997), Evidence for deep mantle circulation from global tomography, *Nature*, *386*, 578–584, doi:10.1038/386578a0.

Verhoeven, O., A. Mocquet, P. Vacher, A. Rivoldini, M. Menvielle, P.-A. Arrial, G. Choblet, P. Tarits, V. Dehant, and T. Van Hoolst (2009), Constraints on thermal state and composition of the Earth's lower mantle from electromagnetic impedances and seismic data, *J. Geophys. Res.*, *114*, B03302, doi:10.1029/2008JB005678.

Wentzcovitch, R. M., B. B. Karki, M. Cococcioni, and S. de Gironcoli (2004), Thermoelastic properties of $MgSiO_3$-perovskite: Insights on the nature of the Earth's lower mantle, *Phys. Rev. Lett.*, *92*, 018501, doi:10.1103/PhysRevLett.92.018501.

Williams, Q., and E. Knittle (2005), The uncertain major element bulk composition of the Earth's mantle, in *Earth's Deep Mantle: Structure, Composition and Evolution*, *Geophys. Monogr. Ser.*, vol. 160, edited by R. Van der Hilst et al., pp. 189–202, AGU, Washington, D. C.

Williamson, E. D., and L. H. Adams (1923), Density distribution in the Earth, *J. Wash. Acad. Sci.*, *13*, 413–428.

F. Cammarano, Institute of Geophysics, ETH Zurich, Hönggerberg, HPP O9, CH-8093 Zürich, Switzerland.

L. Cobden, Department of Earth Sciences, Utrecht University, NL-3584CD Utrecht, Netherlands. (laura@geo.uu.nl)

J. A. D. Connolly, Institute of Mineralogy and Petrography, ETH Zurich, Claussiusstrasse 25, CH-8092 Zürich, Switzerland.

K. Gallagher, Géosciences Rennes, Université de Rennes 1, Campus de Beaulieu, F-35042 Rennes, France.

S. Goes, M. Ravenna, and E. Styles, Department of Earth Science and Engineering, Imperial College London, London, SW7 2AZ, UK.